Applied Catalysis B: Environmental 110 (2011) 14–24

Contents lists available at ScienceDirect

Applied Catalysis B: Environmental

journal homepage: www.elsevier.com/locate/apcatb

An experimental and modelling investigation of the effect of the flow regime on the photocatalytic degradation of methylene blue on a thin film coated ultraviolet irradiated spinning disc reactor

Irina Boiarkina [a], Simon Pedron [b], Darrell A. Patterson [a,c,*]

[a] Separation and Reaction Engineering, Department of Chemical and Materials Engineering, University of Auckland, Private Bag 92019, Auckland Mail Centre, Auckland 1142, New Zealand
[b] Technische Universität München, Fakultät für Chemie, Lehrstuhl 1 für Technische Chemie, Germany
[c] Department of Chemical Engineering, University of Bath, Claverton Down, Bath BA2 7AY, United Kingdom

ARTICLE INFO

Article history:
Received 17 May 2011
Received in revised form 9 August 2011
Accepted 11 August 2011
Available online 30 August 2011

ABSTRACT

In this work, the impact of wave regime and operational parameters on the photocatalytic degradation of methylene blue was investigated on a thin film coated ultra-violet spinning disc. In the employed experimental setup, the wave regimes of spiral, unstructured and crisscross waves as well as smooth film could be observed at disc rotational speeds of 50–200 rpm and flow rates of 5–20 mL/s with a calculated average thickness of 160–450 μm. The glass discs were coated with anatase TiO_2 by a sol–gel procedure followed by heat treatment at 500 °C for 1 h. The reactor was irradiated by a low pressure mercury UV lamp producing an irradiance of 12–23 W/m^2 on the disc surface. The reactant was saturated with oxygen and the effect of spinning speed, flow rate and the resulting wave regime on the degradation rate and kinetics of methylene blue and its reaction intermediates determined. Reactions followed pseudo-second-order kinetics, suggesting dimerisation and/or mass transfer limitations given that the two reactions with the highest conversion observed at 15 mL/s and 100 and 200 rpm, were pseudo-first-order. The spinning disc reactor was, however, not photon transfer limited. The wave regimes showed no impact on the reaction rate, since the flow was mainly laminar with no interfacial mass transfer of oxidant required.

1. Introduction

Photocatalytic degradation of pollutants in wastewaters, employing light and a semiconductor catalyst, has received significant attention in the last three decades [1] due to its ability to fully mineralise a wide variety of compounds. However the industrial applications have remained limited due to the slow kinetics and difficulty in scale up [2–4]. Investigating the use of fixed thin film catalysts has become more popular to overcome the post separation step required with powders, however this results in mass transfer limitations.

One area which has gained considerable interest over the past few years is process intensification. The principal targets of this strategy are to improve efficiency and productivity, reduce the capital cost of process systems, improve their intrinsic safety and minimise their environmental impact [5,6]. A spinning disc reactor (SDR) is one such technology, whereby a liquid is fed onto the centre of a horizontally rotating disc, causing it to spread out into a very thin film with thicknesses in the order of 20–200 μm [7,8]. The high centrifugal acceleration causes the films to be highly sheared and this reactor shows enhanced heat and mass transfer characteristics [7,9,10], which makes the SDR of interest for mass transport limited reactions [7]. The thin film thickness is well controlled by these reactors, allowing high ultraviolet (UV) penetration of the photocatalyst throughout the liquid, potentially opening up photocatalytic reactions to more highly coloured, turbid liquids. A short and narrow residence time distribution is an attractive attribute for liquid–solid reactions such as the radical polymerisation of styrene [7] and crystallisation of pharmaceuticals [5].

Several flow regimes can form on the surface of the disc, depending on the liquid's physical properties, the flow rate and rotational speed. The flow regimes change from smooth to concentric waves, spiral waves, irregular waves and film break-up [8]. There have been few experiments investigating whether the flow across the spinning disc is laminar or turbulent in nature, however Butuzov and Pukhovoi found, through dye injection studies, that several flow regime zones formed across the surface of the disc. The first is the injection zone where the liquid is being accelerated to the rotational speed of the disc, followed by the turbulent acceleration zone, finally the flow becomes laminar in nature again towards the edge of the disc [11].

* Corresponding author. Tel.: +64 9 373 7999; fax: +64 9 373 7463.
E-mail addresses: darrell.patterson@auckland.ac.nz, d.patterson@bath.ac.uk (D.A. Patterson).

0926-3373/$ – see front matter © 2011 Elsevier B.V. All rights reserved.
doi:10.1016/j.apcatb.2011.08.008

Nomenclature

ν	kinematic viscosity ($m^2\ s^{-1}$)
ρ	density ($kg\ m^{-3}$)
ω	rotational speed of spinning disc ($rad\ s^{-1}$)
Q	volumetric flow rate ($m^3\ s^{-1}$)
h	height of the liquid film at radius r (m)
R_i	reaction rate (mol/L s)
C	concentration of substrate (mol/L)
C_0	initial concentration of substrate (mol/L)
V	reactor volume (m^3)
S	illuminated surface area of catalyst (m^2)
$k_{app,\nu}$	pseudo-first or second order reaction rate constant based on reactor volume (s^{-1} or $m^3\ mol^{-1}\ s^{-1}$)
$k_{app,s}$	pseudo-first or second order reaction rate constant based on surface area (m/s^1 or $m^4/mol\ s$)
$\phi_{overall}$	overall quantum yield
ξ	photon efficiency
E	Ekman-number
A	Nusselt film height equation constant ($m^{5/3}$)
R	outer disc radius (m)
R_0	inlet nozzle radius (m)
I_0	irradiance before absorption (W/m^2)
I	irradiance after absorption (W/m^2)
ε	molar absorptivity of the absorbing species ($L\ mol^{-1}\ m^{-1}$)
l	the path length through the material containing the absorbing species (m)
t	time (s)

The only previous study employing an SDR for photocatalytic treatment of wastewater is by Yatmaz et al. [12], who investigated the degradation of 4-cholorophenol and salicylic acid using titanium dioxide as the photocatalyst. They focused on evaluating the performance of the reactor based on the UV irradiation source and found that shorter wavelengths were better. They did not investigate the effect of flow regime or operational parameters on the reaction rate.

The aim of this work is to fill this gap and evaluate the performance of an SDR as a photocatalytic process intensification technology and establish whether the wave regimes and operational parameters affect photocatalytic degradation of methylene blue. Methylene blue was chosen since it has well established kinetics and reaction mechanisms in conventional photocatalytic reactors, which can be used to benchmark the SDR performance against [13]. As titanium dioxide is a well-established photocatalyst, the experiments will be carried out with a TiO_2 coated glass disc.

2. Materials and method

2.1. Materials

Pure azure A and B were obtained from Acros Organics and the methylene blue was obtained from Sigma–Aldrich (85% pure). 99.5% pure oxygen by BOC gases was used for saturation of the reactant solution.

The reagents used for TiO_2 sol preparation were glacial acetic acid (Univar, 99.7%), acetylacetone (Sigma–Aldrich, 99%), isopropanol (Univar, 99.7%), titanium isopropoxide (Aldrich, 97%) and deionised water (from an ELGA Maxima Ultra purifier system). All reagents were used as received.

2.2. Analytical methods

The degradation of methylene blue was analysed using a Shimadzu LC-20AT high performance liquid chromatography (HPLC) instrument with an SPL-20A UV–vis detector and an Agilent Eclipse XDB-C18 column. A gradient method was used where solvent A comprised of deionised water with 0.1(v/v)% trifluoroacetic acid (Sigma–Aldrich, 99%) and solvent B comprised of 0.01(v/v)% trifluoroacetic acid, 80(v/v)% acetonitrile (Merck, 99.8%) and 20(v/v)% deionised water. A detection wavelength of 662 nm was used. The gradient method employed was 95% solvent A at 0 min, 90% solvent A at 5 min, 10% solvent A at 40 min and 95% solvent A at 45 min. A flow rate of 1 mL/min was used with an injection rate of 50 μL, oven temperature of 25 °C and total analysis time of 50 min. The method was based on the work of Ali et al. [3].

The UV light intensity was measured using a SUV 20.IA2Y2 photometer by IML, which was connected to a TENNA 72-7765 multimeter.

2.3. Catalyst immobilisation

The sol–gel coating process was used to immobilise the titanium dioxide on the surface of the glass discs. The sol was made according to the method described by Ling et al. [14]. The glass discs were extracted from the sol at 1 mm/s, allowed to air dry for 5 min in the fume-hood and then transferred to an oven at 100 °C for 30 min. This process was repeated once more before the discs were transferred to a furnace (F.E. Kiln with an RTC 1000 Bartlett Instruments Co. controller) for calcination at 500 °C for 1 h to obtain the photocatalytically active anatase crystal structure. The furnace was ramped up at a rate of 2 °C/min to minimise cracking. Once the discs had cooled the process was repeated once more to obtain a total of four TiO_2 layers, of which two were calcined.

2.4. Experimental setup and procedure

A process flow diagram of the experimental setup is shown in Fig. 1a. The experiment was run in batch mode. The reactant was pumped from a stirred tank reservoir, a 500 mL glass beaker, to the reactor with total recycle and was oxygenated at a flow rate of 450 mL/min. The employed norprene (Masterflex 064042) piping had an inner diameter of 8 mm. The liquid was pumped with a peristaltic pump (Cole-Parmer, 7553-75) from the stirred tank into a tightly sealed glass flask, which acted as a buffer to dampen the flow pulsations. The beaker and buffer flask were wrapped with aluminium foil to prevent photolysis of methylene blue. The liquid was cooled with tap water with a Liebig cooler before entering the reactor from below. The SDR was specially built on-site at the University of Auckland. The inlet design was different from reactors used in the past in that the inlet pipe came in from the bottom of the reactor and went through the centre of the shaft (for rotating the disc) before coming out of the centre of the disc. This was to ensure no shadowing of the UV light, which would have been unavoidable with the more traditional top feed tube. The inlet nozzle diverted the flow, so that the liquid hit the disc from above at a radius of 21 mm through an annular-shaped gap. The disc diameter was 200 mm. The whole SDR was enclosed in an UV tight enclosure to ensure no exposure to the operators. The reactor lid was fitted with a low pressure mercury UV lamp inside a quartz tube (20 W, monochromatic, $\lambda = 254$ nm, Steriflow, supplied by Davey Water Products NZ, part nr. GPH369N/S), with the lamp being situated at the focus of a parabolic mirror to improve the homogeneity of the irradiation. After reaction, the liquid was collected in a basin below the disc. The reactor was situated above the stirred tank, so that it could return back by gravity to the stirred reactant reservoir. Photographs of the experimental setup are shown in Fig. 1.

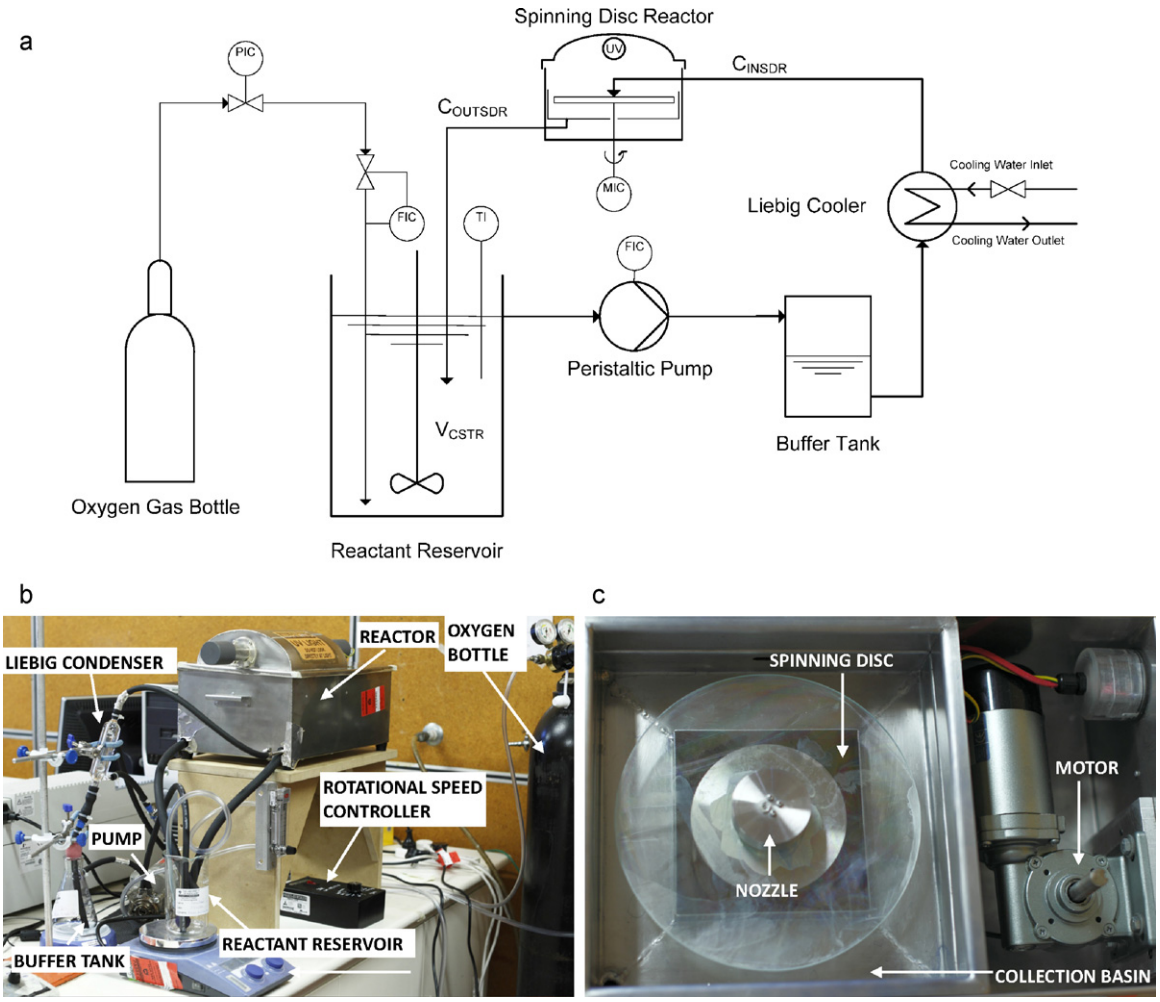

Fig. 1. Photographs of the employed experimental setup (a) process flow diagram of the thin film photocatalytic SDR, (b) overall experimental assembly and (c) inside the reactor.

The employed reactant volume was 550 mL of aqueous 10 mg/L (26.74 μmol/L) methylene blue solution. Of it, 150 mL was poured into the buffer tank (Fig. 1a) before starting the experiment. The buffer flask was closed so as to be gas-tight. The remaining liquid was poured into the stirred reservoir (Fig. 1a). The desired rotational speed of the disc was adjusted. In order to blow out any air bubbles in the nozzle, a flow rate of 35 mL/s was used for 20 s before re-setting to the desired flow rate. The reactor was then closed with the lid.

The setup was run for 20 min in the dark to allow for the adsorption of methylene blue to reach equilibrium, before the lamp was switched on and the reaction started. The reactor was run for 3 h. The temperature of the reactant was kept at 27 ° C during the reaction.

The error was calculated from the average standard deviation of repeat experiments and was used to plot the error bars in the figures.

3. Modelling

3.1. Reaction kinetics

It is generally agreed that the main reaction mechanism defining the photomineralisation of organic compounds with O_2 on TiO_2 is of the Langmuir–Hinshelwood type (Eq. (1)). It successfully describes the reaction rate of several species between substrate and hydroxyl radical with at least one species adsorbed on the catalyst surface [1,15,16].

$$R_i = -\frac{dC_0}{dt} = k\theta = \frac{kKC_0}{1+KC} \quad (1)$$

where R_i is the rate of substrate removal, C_0 is the initial substrate concentration, θ is the surface coverage, t is the reaction time, K is the Langmuir adsorption constant of the substrate and k is a proportionality constant which quantifies the intrinsic reactivity of the photoactivated surface with the substrate.

K is therein not identical with the dark Langmuir adsorption isotherm for the substrate on the semiconductor; the latter values are usually much smaller. k is found to be dependent on light intensity and correlating with the fraction of O_2 adsorbed on the catalyst surface [1]. For high concentrations of substrate, the degradation is pseudo-zero order. For low concentration reactions which are not oxygen limited, the reaction is pseudo-first order. In this case, the kinetics are described by Eq. (2)[15,17].

$$R_i = k_{app,v}C_0 \quad (2)$$

where $k_{app,v}$ is the pseudo-first-order reactor volume based reaction rate constant, which encompasses the rate of light absorption as well as the oxidant and catalyst concentration. Side reactions are supposed to occur slowly and have to be taken into account only at higher conversions [17]. The surface area based reaction rate

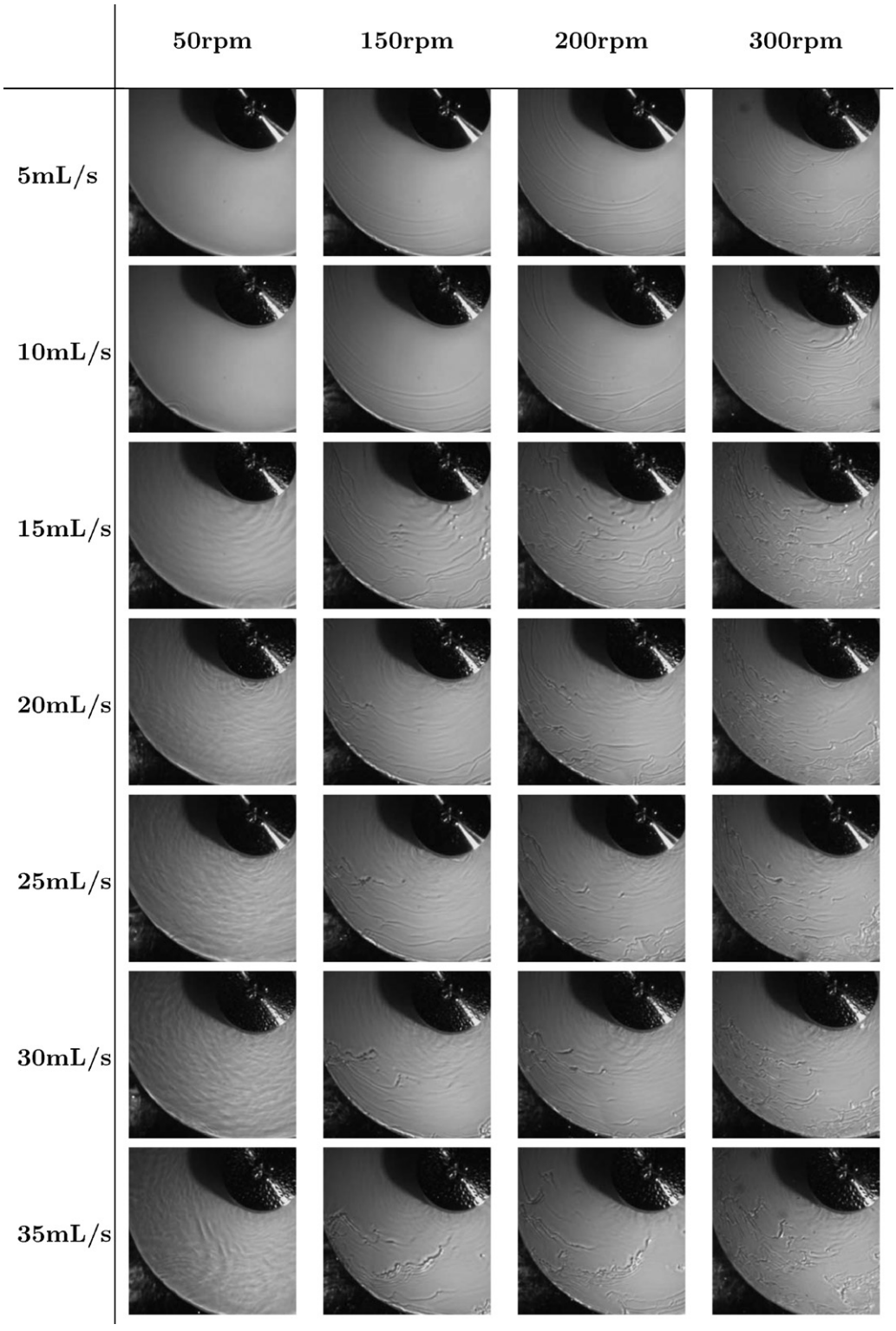

Fig. 2. High speed camera images of the spinning disc fed water at various flow rates and disc rotational speeds.

constant can be calculated from the volume reaction rate constant using Eq. (3).

$$k_{app,s} = \frac{V}{S} k_{app,v} \tag{3}$$

where S is the illuminated surface area of the catalyst and $k_{app,s}$ is the pseudo-first or second order reaction rate constant.

The efficiency of the photoreaction can be described by the overall quantum yield, $\phi_{overall}$, which is defined in Eq. (4)

$$\phi_{overall} = \frac{\text{rate of reaction}}{\text{rate of absorption of radiation}} \tag{4}$$

However, the rate of photon absorption is difficult to measure, thus an alternative parameter, the photon efficiency, ξ, is preferred. It is defined for monochromatic light as the number of transformed

molecules divided by the number of photons incident from the UV light source and has been used in this work [1,15].

$$\xi = \frac{\text{reaction rate}}{\text{incident monochromatic light intensity}} \quad (5)$$

3.2. Flow modelling across the disc

In order to be able to model the SDR, the film height distribution across the surface needs to be known. For simplicity, the Nusselt model is the most commonly used. This model assumes fully developed laminar flow across the surface of the disc with no shear at the gas–liquid interface. One of the implied assumptions with fully developed flow is that the liquid hitting the disc surface reaches the disc rotational speed instantaneously: there is no accelerative zone. Hence, this model works best with viscous Newtonian fluids. The mean film thickness as derived by the Nusselt model is given in Eq. (6)[9,18]. The film thickness, as predicted by the Nusselt formula, generally over predicts the film height and does not account for surface waves. Though since it is in the same order of magnitude, it would be a good indicator of the expected film thickness. There are other models for modelling the film height, such as that presented by Charwat et al. [8] or Matar et al. [19], however they are either empirical (and hence the validity has to be questioned for a different reactor setup) or complex to solve.

$$h_N = \left(\frac{3Q\nu}{2\pi r^2\omega^2}\right)^{1/3} \quad (6)$$

The Ekman number, Eq. (7), characterises the ratio of the viscosity to the coriolis force.

$$E = \frac{\nu}{\omega h^2} \quad (7)$$

For $E > 10$, the film thickness can be approximated by the Nusselt model. However, for low values of E, inertial contributions dominate and the film thickness deviates markedly from the Nusselt model [8,9]. In the current work the Ekman number range of the experiments was between 1.8 and 7.2, which although are lower than the cut off, are still on the same order of magnitude. This means that there will be some error in the film thickness estimated using Eq. (6).

3.3. Overall reactor modelling

A mass balance can be performed on the system by treating the reactor and the substrate reservoir separately, as shown in Fig. 1a. The reactant reservoir is assumed to behave like an ideal stirred tank; perfect mixing and the outlet concentration equal to the bulk volume concentration. This leads to the expression shown in Eq. (8).

$$\frac{dC_{INSDR}}{dt} = \frac{Q}{V_{CSTR}}(C_{OUTSDR} - C_{INSDR}) \quad (8)$$

For modelling the flow across the disc the local film thickness is calculated with the Nusselt formula presented in Section 3.2, which can be rearranged into the form shown below, Eq. (9). The constants have been combined into one variable, A, for simplicity:

$$h(r) = Ar^{-2/3} \quad (9)$$

Assuming that the SDR behaves like a plug flow reactor, which is a good assumption if the flow is shown to be laminar, with no mass transfer resistance to the disc surface leads to the following expression for the change in concentration with respect to radius:

$$\frac{dC}{dr} = \frac{2\pi A}{Q} r^{\frac{1}{3}} R_i \quad (10)$$

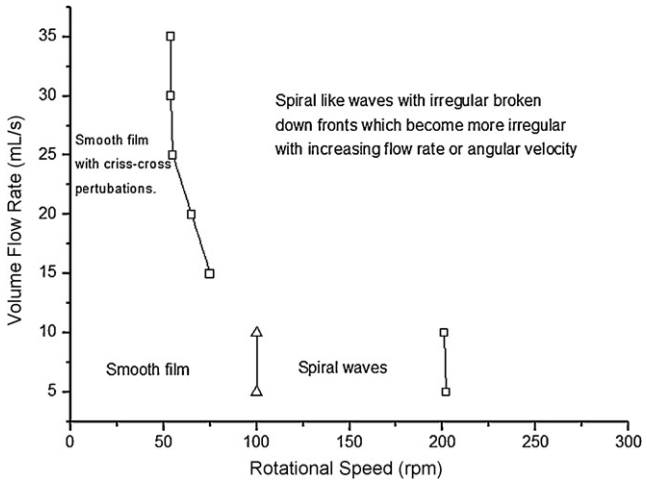

Fig. 3. Flow regimes on the spinning disc reactor at different flow rates and rotational speeds.

where R_i is the reaction rate. For a pseudo-first order reaction $R_i = -kC$ and can be solved analytically, in combination with Eq. (8) to yield the following expression for the change of concentration with respect to time in the reactant reservoir:

$$C = C_0 \exp\left(\frac{Q}{V}\left[\exp\left(-\frac{3\pi Ak}{2Q}(R^{4/3} - R_0^{4/3})\right) - 1\right]t\right) \quad (11)$$

where R is the outer radius of the disc and R_0 is the inlet nozzle radius. A plot of $\ln(C/C_0)$ versus time should yield a straight line relationship for a pseudo-first order reaction and allow for the calculation of the reaction rate constant.

However, Rauf et al. [20] found that the degradation of methylene blue followed pseudo-second order kinetics possibly due to the dimerisation of the methylene blue. For a pseudo-second order reaction $R_i = -kC^2$. Substituting this into Eq. (10) leads to Eq. (12), however when the integrated result of this is substituted into Eq. (8), the final reactor model cannot be solved analytically.

$$\frac{dC}{dr} = -\frac{2\pi A}{Q} r^{1/3} kC^2 \quad (12)$$

Eq. (12) was therefore solved and fitted iteratively with Eq. (8) to experimental data in MATLAB. In modelling the reactor in this way, it is assumed that no reaction occurs in the pipes and buffer connecting the reactor to the reactant reservoir. This assumption is good, since significant reaction rates should not occur in the absence of both UV irradiation and photocatalyst.

4. Results and discussion

4.1. Study of flow regimes

Flow regimes are peculiar to the type of SDR. Since this SDR is unique, the flow characteristics of the spinning disc and liquid film needed to be characterised.

On the spinning disc, flow regimes were investigated for flow rates of 5–35 mL/s and rotational speeds of 50–400 rpm with water only. The high-speed camera image stills are shown in Fig. 2 and an overview of the boundaries between the observed wave regimes is given in Fig. 3. The defined boundaries in Fig. 3, which show the transition from smooth to spiral, or smooth to unstructured means that at those conditions, the first spiral or unstructured waves respectively were observed when the rotational speed was increased.

The transition between spiral and unstructured was difficult to define, as the unstructured waves still possessed some form of

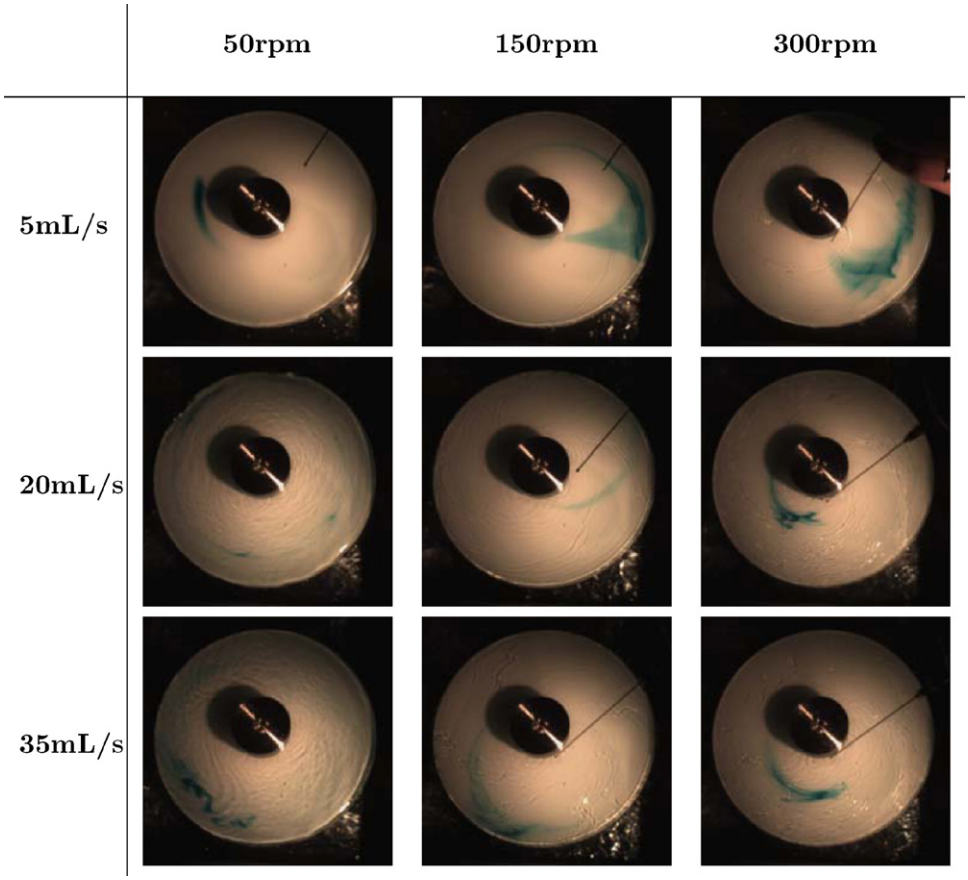

Fig. 4. High speed camera images of the spinning disc with dye injected at the inlet.

spiral element in them. What was characterised as "unstructured" meant that the spiral front was broken down, from its initial smooth front. Therefore an increase in either the flow rate or rotational speed caused the spiral front to be more irregular in shape. This can be seen clearly in Fig. 2 when the flow rate is adjusted from 10 mL/s to 15 mL/s at 150 rpm.

Under the examined conditions, no film break-up was observed, which was expected, as the minimum absolute layer thickness achieved according to the Nusselt model was 82 μm, thus higher than that required for film break up (20 μm, as found by Charwat et al. [8]). Concentric waves could not be observed in the range where they were observed by Charwat et al. [8]. This might be due to strong inlet effects on the disc caused by the nozzle design.

At low flow rate and rotational speed, a smooth film covered the disc with accumulation occuring at the disc edge, shown in Fig. 2 at flow rates of 5 and 10 mL/s and spinning speed of 50 rpm. However, even at the lowest flow rate, liquid drops falling off the spinning disc caused perturbations of the liquid film by being point sources of waves on the disc's edge which propagated inward to the disc centre. At flow rates higher than 15 mL/s, the smooth film was additionally perturbed by nozzle inlet effects, which acted as point sources for waves propagating outward on the disc. Compared to images of spinning disc experiments at the same flow conditions from literature, the latter effect was very prominent as the disc employed in this work had a significantly smaller diameter [8,18,21]. These inlet and outlet perturbations caused crisscross waves to perturb the surface at flow rates above 15 mL/s (Fig. 2), across the entire studied range of rotational speeds. This may at least in part explain the differences in flow regimes to others in the literature.

It was observed that generally the liquid film close to the disc's centre was smooth and, depending on the flow rate, with or without inlet perturbations. Increasing the rotational speed at constant flow rate resulted in the transition from a smooth film to spiral or unstructured waves, which propagated from the edge of the disc towards the centre (Fig. 2: 10 mL/s, change from 50 rpm to 150 rpm and 300 rpm).

The transition between any two wave regimes was clearly visible for flow rates equal and lower than 10 mL/s. For flow rates higher than 10 mL/s, the smooth film at low rotational speed was totally perturbed by crisscross waves and the nature of the spiral waves became less clear.

The distance between the wave fronts decreased with increasing rotational speed. From the images, the amplitude of the waves cannot clearly be deduced.

Ink injection experiments at 5, 20 and 35 mL/s and 50, 150 and 300 rpm revealed that the liquid film for all observed flow regimes under the observed conditions appeared laminar; clear, well defined streaklines of the injected dye can be seen in Fig. 4. The injected dye follows the wave fronts sharply, as shown in Fig. 4 at 5 mL/s and 300 rpm, and 35 mL/s and 50 rpm; the waves do not seem to contribute to the mixing outside of diffusion. Fig. 4 5 mL/s and 150 rpm shows diffusion and the dye injected fluid volume being stretched as the film thickness decreases going across the radius of the disc.

Fig. 4 (for example 50 rpm and 35 mL/s, 300 rpm and 5 mL/s) shows the dye following the wave fronts – without significant mixing in front. The streaklines are sharp, such as those visible for 300 rpm and 35 mL/s, 150 rpm and 5 mL/s in Fig. 4. No significant dye mixing was observed, however any "micro" mixing within the generated dye streaklines would not have been visible.

The photocatalytic experiments were run at flow rates of 5–20 mL/s and rotational speeds of 50–200 rpm, as all observed flow regimes were represented in this experimental range.

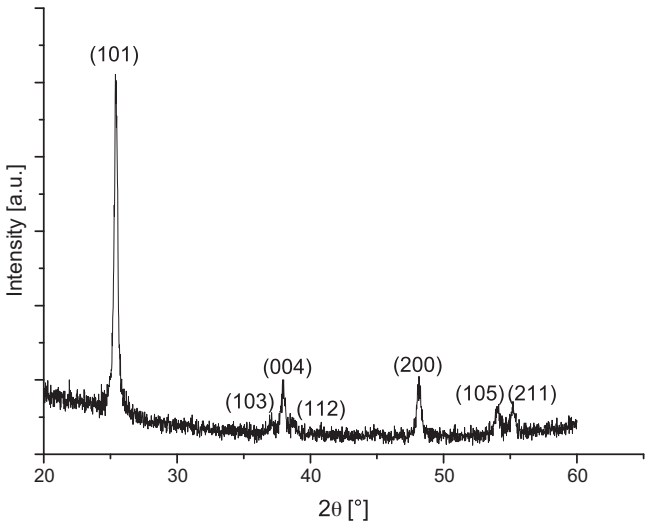

Fig. 5. XRD spectrum of the TiO_2 coating.

Note that these wave regimes are observed and filmed in the absence of UV light. There is evidence that the TiO_2 surfaces become more hydrophilic when irradiated by UV light due to band-gap excitation [22]. This effect may have some influence on the flow regimes during reaction that are not measured in this non-UV light exposed analysis. However, any differences in flow regimes cannot be precisely quantified, since it is impossible to film the flow regimes on the disc when it is irradiated with UV light in the reactor enclosure used as the high speed camera employed in this work is too large. However, since the disc is always fully covered with a film of fluid when exposed to UV light, the loss of intensity through the liquid film would minimise the change in surface energy, possibly minimising any significant influence on the wave regime.

4.2. Characterisation of the TiO_2 film

The TiO_2 coating from sol–gel deposition was imaged by SEM and by X-ray diffraction. The X-ray diffraction spectrum is shown in Fig. 5 and the spectrum shows characteristic TiO_2 anatase peaks according to the standard spectrum JCPDS #84-1286 and [23]. No rutile peaks are present.

Fig. 6 shows SEM images of the TiO_2 film before and after reaction; no clear catalyst degradation is observed. The texture of the film is non-porous and the cross-sectional images (Fig. 6a and b) show that the film is coherently attached to the surface of the glass discs.

4.3. Kinetics of the degradation of methylene blue

4.3.1. Control experiments

Control experiments (Fig. 7a) showed that methylene blue does not react with UV light and without TiO_2 in the employed reactor confirming the assumption made in Section 3.3. This comparatively slow photolysis rate was similarly found by Houas et al. [24] and Ali et al. [3]. Quantifiable adsorption of methylene blue in the system takes place only in the first 20 min of the reactant solution in the reactor. The uncatalysed photolytic degradation of methylene blue was thus found to be negligible and was not accounted for during the modelling of the reactor.

4.3.2. Thin film photocatalysis of methylene blue in the SDR

During reaction, the identified intermediates were azure A and azure B. As the kinetics of methylene blue degradation were found to be independent of the intermediates' concentration, a detailed

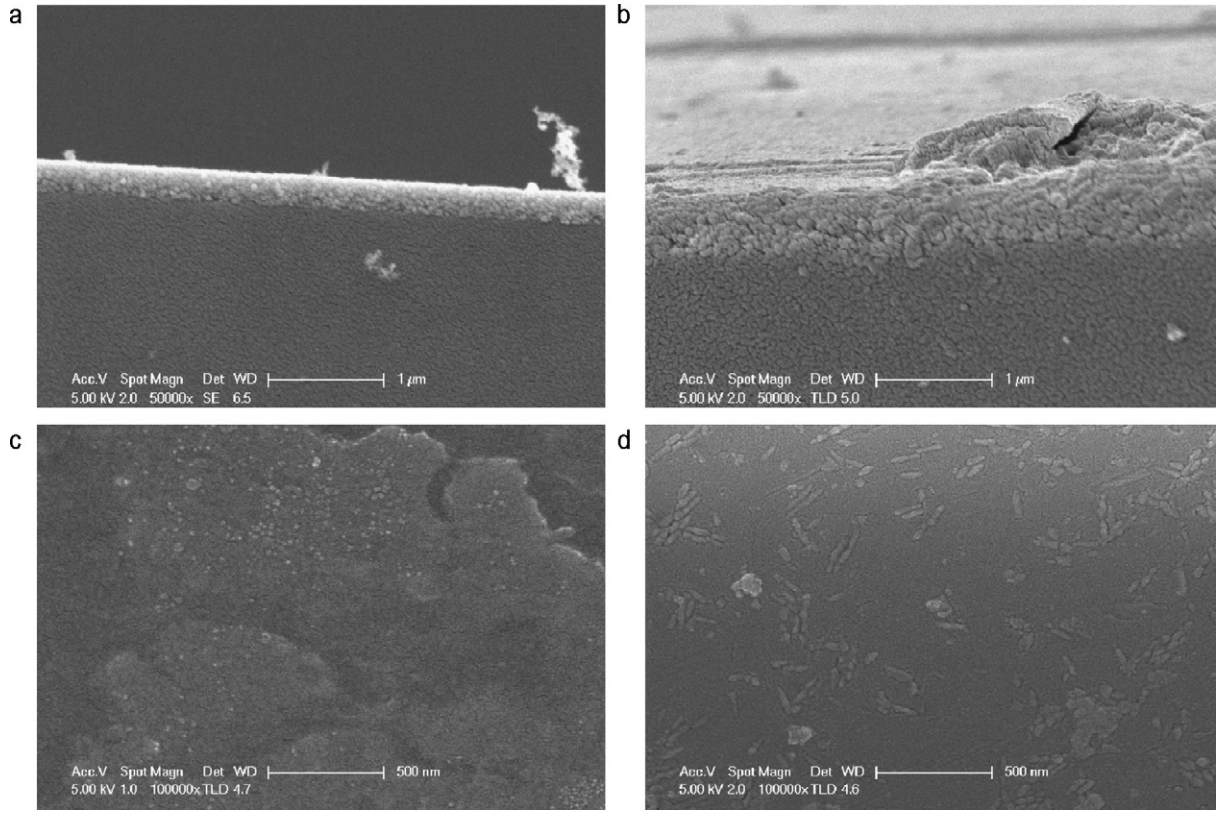

Fig. 6. SEM images of titanium dioxide sol–gel coating: (a) cross-sectional view before reaction (b) cross-sectional view after reaction (c) front on view before reaction (d) front on view after reaction.

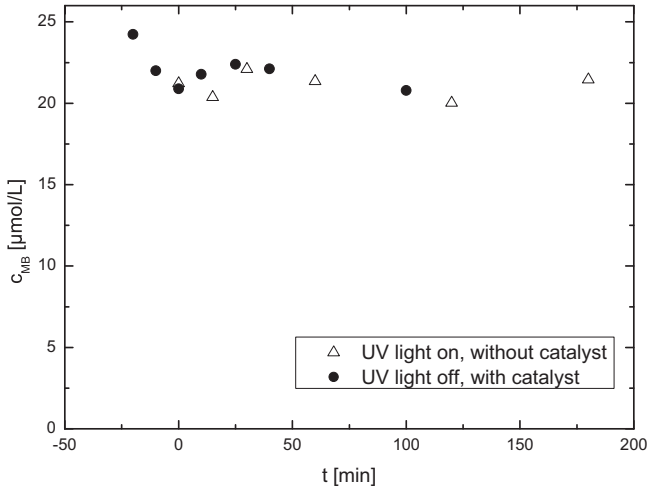

Fig. 7. Example concentration vs. time plots of methylene blue degradation (a) with catalyst and no UV and without catalyst but with UV (b) pseudo-first order – 15 mL/s, 200 rpm (c) pseudo-second order reaction – 20 mL/s, 200 rpm.

photocatalytic reaction pathway analysis will not be presented here.

In heterogeneous catalysis with immobilised catalyst, the kinetics can also be expressed on a UV light irradiated surface area basis (Eq. (3)). The effect that there is a different reaction volume per surface area ratio at different flow conditions in the SDR can thereby be computationally eliminated. However, it should be noted that the surface area used is the illuminated surface area, not the surface area of the catalyst; the surface area of the catalyst in this configuration is difficult to quantify and will vary based on the quality of the coating from disc to disc, which will contribute to an increase in the scatter of the data.

Kinetic analysis of the methylene blue concentration versus time data showed that the degradation of methylene blue mainly followed pseudo-second order reaction kinetics – example concentration versus time plots are shown in Fig. 7. The surface reaction rate constants are shown in Fig. 8a. In this, two maxima become evident: the data points at 15 mL/s. However, those reactions followed pseudo-first order kinetics. The fitted pseudo-first order surface area reaction rate constants are given in Table 2, as distinct from the pseudo-second order rate constants detailed in Table 1. The average error confirms that the 15 mL/min reaction rates were real data points that were significantly higher than expected.

Fig. 8a also shows that the surface reaction rate is otherwise independent of the film height, again showing that the reaction is not photon transfer limited. However, when calculating the reaction rate on a volume basis (Fig. 8b), it can be seen that the reaction

Table 1
Pseudo-second order rate constants and average liquid film heights $\bar{h}$ of the pseudo-second order reaction experiments.

Q (mL/s)	ω (rpm)	Wave regime	$k_{app,s} \times 10^4$ ($m^4\ mol^{-1}\ s^{-1}$)	$\bar{h}$ (µm)
5	50	Smooth	3.45	283
5	100	Smooth	1.92	178
5	200	Helical	1.65	112
5	200	Helical	1.70	112
10	50	Smooth	1.58	356
10	150	Helical	2.69	171
20	50	Crisscross	1.81	449
20	50	Crisscross	0.97	449
20	150	Solitary	2.18	216
20	200	Solitary	1.16	178
20	200	Solitary	2.06	178
20	200	Solitary	2.49	178

Table 2
Pseudo-first order rate constants and average liquid film heights of 15 mL/s experiments.

Q (mL/s)	ω (rpm)	$k_{app,s} \times 10^6$ (m/s)
15	100	8.85
15	200	8.92

rate decreases with increasing film height. This implies that the reactor volume increases with increasing film height, approximately the same quantity of molecules still get degraded per unit surface area. This implies that the best reaction conditions become the highest flow rate for the same film height as the residence time decreases, thus recycling unreacted molecules to the surface faster. This can be achieved by increasing the rotational speed. However, the 15 mL/s reactions are the exception to this, implying that another effect is taking place.

In order to compare reactions of different orders, the reaction rates at 26 µmol/L and 13 µmol/L are shown in Figs. 9a and b respectively. It becomes evident that in the observed concentration range, the two pseudo-first order reactions show higher reaction rates and thus higher conversions after a specified time than pseudo-second order reactions. The lower the concentration of substrate, the higher is the difference between first- and second order reaction rates. A change in reaction mechanism occurs from pseudo-second to first order, which is enhancing the reaction kinetics.

Fig. 10 shows a slight local reaction rate maximum at 5 mL/s and 50 rpm, which can be explained by the slightly inaccurate modelling of the reactor volume on the disc with the Nusselt film thickness model; in reality there was visible accumulation of liquid at the disc's edge, enlarging the reaction volume. Also, the liquid film on the SDR did not exhibit clear turbulent flow characteristics in the range of the tested parameters. However, it is possible that special fluid dynamic effects take place when the wave regime changes from helical waves at lower flow rates to unstructured (Fig. 3). Further investigation is required to confirm this.

In literature, only cases of pseudo-first order photocatalytic decomposition of methylene blue at similar concentrations as used in this work and employing pure TiO_2 as photocatalyst are reported. However, Rauf et al. [20] found pseudo-second order kinetics for the photocatalysed degradation of methylene blue on Cr–Ti binary oxide with 10% molar Cr^{3+} content (Ti–10Cr). They explained the kinetics of their experiments with the tendency of methylene blue to aggregate or dimerise antecedent to the photochemical reaction due to strongly attractive electrostatic forces between the ionic dye molecules with increasing methylene blue dye concentration [25]. On the other hand, the results of Ghandazadeh et al. [25] reveal that dimerisation and aggregation become less significant at decreasing concentration and thus the reaction gets mainly monomolecular. However in the current work all the starting concentrations used were equal, therefore it is more likely that an enhancement of mass transfer is occurring at 15 mL/s.

A plot of the reaction rate constant over the average height of the SDR liquid film, Fig. 10, shows that wave regimes do not have an influence on the reaction kinetics. The two points at maximum reaction rate are in the unstructured wave regime, the other point assigned to unstructured wave regime lies within the range of the other wave regimes. The rate constant of the experiment at 15 mL/s and 200 rpm on a volume basis is 3.3 min^{-1}, which is 55 times the value detected by Houas et al. [24]. One reason for the enhanced reaction rate is that in this work the reactant solution was consistently saturated with oxygen, meanwhile in the study carried out by Houas et al. [24] the solution was oxygenated through mass transfer with the ambient air, which may have resulted in less than saturated conditions. However, it should be noted that Houas

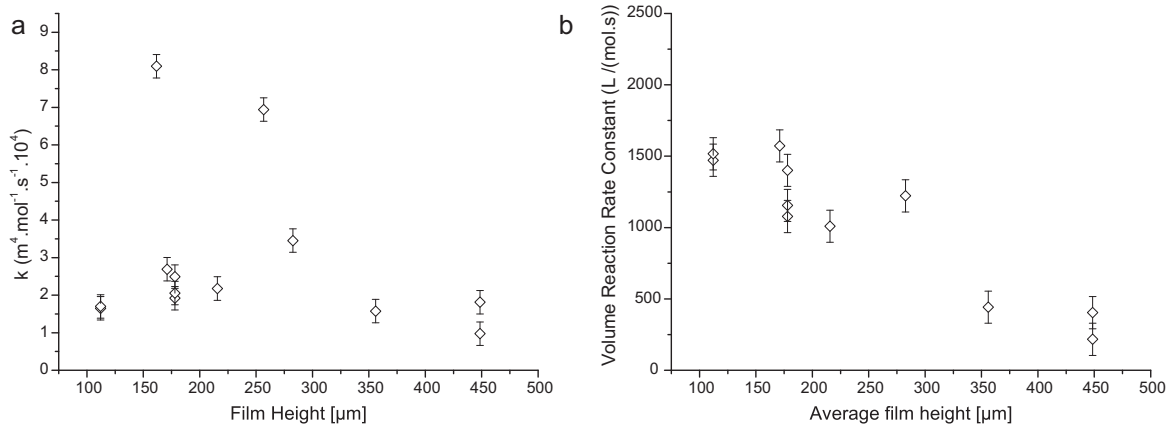

Fig. 8. Effect of film height on the (a) the surface area based pseudo-second order reaction rate constant (b) the volumetric pseudo-second order reaction rate constant (this data excludes the pseudo-first order reactions occurring at 15 mL/s).

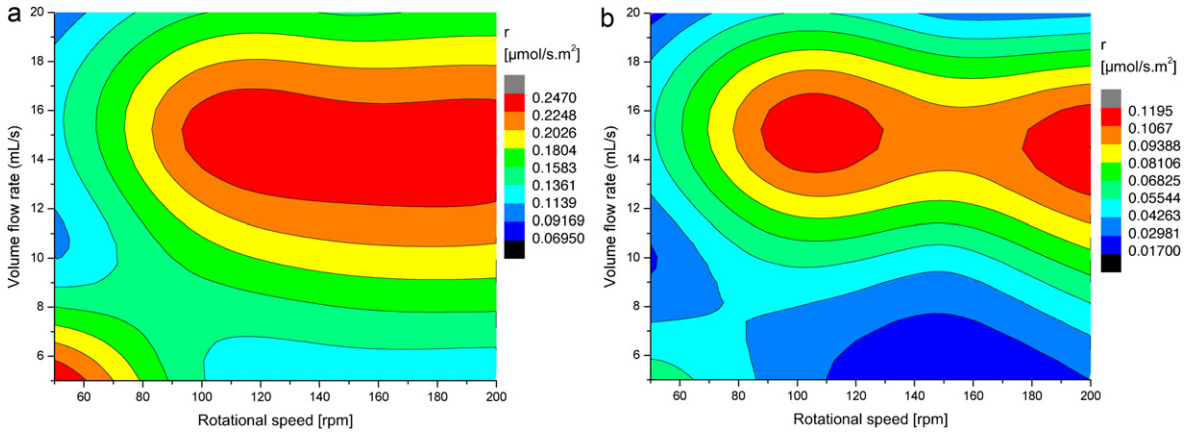

Fig. 9. Calculated reaction rates at methylene blue concentrations of (a) 26 µmol/L and (b) 13 µmol/L.

et al. used a suspension, as opposed to immobilised catalyst, which means the surface area available for reaction would have been significantly larger. The average quantum yield obtained in our reactor at 26 µmol/L was 0.4%, which was higher that found by Houas et al. of 0.14% at the start of the reaction 72 µmol/L, supporting the use of the SDR as a photocatalytic reactor.

4.4. Photon flux and photonic efficiency

The UV irradiance was measured at eight points inside the reactor level at the height of the glass disc's surface. OriginPro 8.1G was used to plot the irradiance distribution profile as shown in Fig. 11. The irradiance profile is symmetric about the UV lamp axis with the

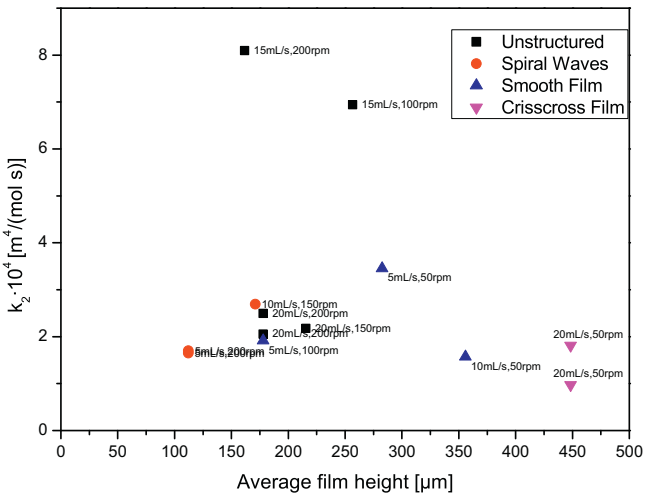

Fig. 10. Effect of film height on the pseudo-second order surface area based reaction rate constants as classified by flow regime.

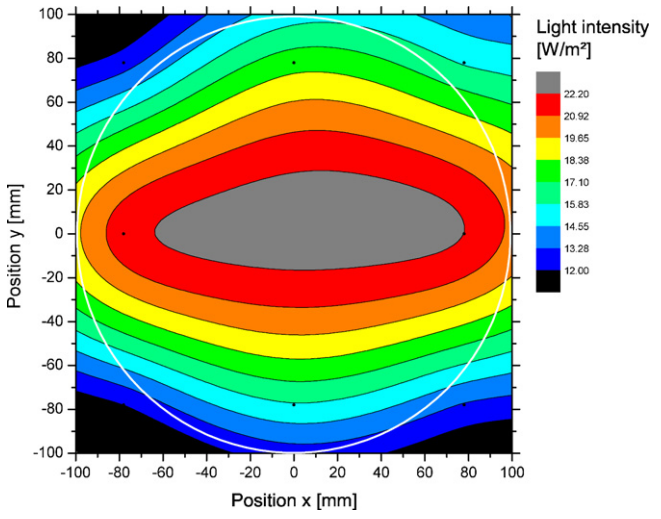

Fig. 11. UV light intensity distribution on the glass disc in the spinning disc reactor, with white circle indicating the outside disc surface.

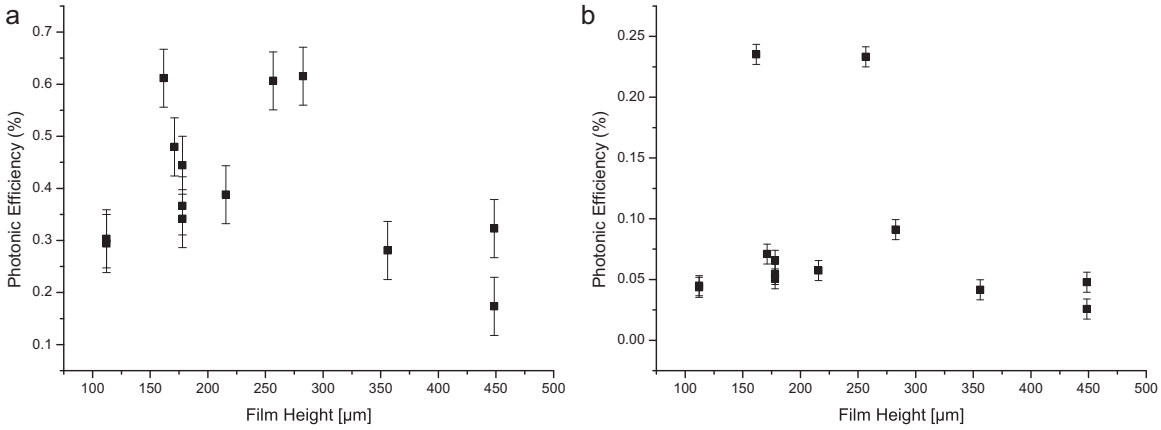

Fig. 12. Effect of film height on photonic efficiency at (a) 26 μ mol/L methylene blue and (b) 10 μ mol/L methylene blue.

maximum occurring at the centre of the disc. The irradiance profile is not completely homogeneous, with the measurements varying between 12 and 23 W/m^2. However, the difference between the maximum and minimum in the same order of magnitude, unlike the results achieved in the work of Dionysiou et al. [26] (albeit with a vertically rotating disc reactor), with values of 0.3–15 W/m^2. The UV irradiation in this work is the most uniform yet for a photocatalytic SDR. The parabolic mirror with the UV lamp in its focus is responsible for the relatively uniform irradiance of the disc.

Fig. 11 and the reaction data were used to calculate the photon flux reaching the catalyst surface and hence the photonic efficiency of the process, which is shown is Fig. 12b. The average photon flux was 3.8×10^{-5} Einsteins/m^{2}s. It can be seen that the photonic efficiency for the process remains approximately constant with the film height, with the exception of two outliers, as shown previously; these are reactions carried out at 15 mL/s and displayed atypically high reaction rates, with reaction order also switching from second to pseudo-first order. The average photonic efficiency, as calculated at a concentration of 10 μmol/L, of 0.054% (excluding the outliers) was comparable to that documented by Tschirch et al. [27] for methylene blue at the same concentration.

The fact that Fig. 12b shows no obvious trend of decreasing photonic efficiency with increasing film height is also a good indication of that the reaction is not photon transfer limited. The Beer–Lambert law, shown below in Eq. (13), can be used to quantify the light irradiance absorbed by the solution.

$$\log_{10}\left(\frac{I_0}{I}\right) = \varepsilon l C \tag{13}$$

where I_0 is the intensity before absorption, I is the intensity after absorption, ε the molar absorptivity of the absorbing species (L mol^{-1} m^{-1}), l is the path length through the material containing the absorbing species (m) and C is the concentration of the absorbing species (mol/L) [2].

If the reaction was photon transfer limited due to strong absorption of light by the methylene blue, then we would expect to see a strong dependence of the photonic efficiency on the film height, which is not apparent. Consequently, the decrease in reaction rate with film height observed in Section 4.3 is not attributable to increasing absorption by the increased film thickness.

The photonic efficiency found by Dionysiou et al. [26] for the degradation of 4-chlorobenzoic acid on a vertically rotating disc photocatalytic reactor was on the order of 2.7%, which is several orders of magnitude higher than that found in this work. This discrepancy can be attributed to several factors, of which the most important is the average reaction rate at which the photonic efficiency is calculated. Eq. (4) shows that the photonic efficiency is calculated from the average reaction rate, however this changes as the reaction proceeds, hence the calculated photonic efficiency is a function of the concentration at which the reaction rate is calculated. Dionysiou et al. [26] calculated their reaction rate based on the number of molecules converted in the first 30 min of the reaction, with a starting concentration of 288 μmol/L. This is an order of magnitude higher than the starting concentration of 10 μmol/L used in this work of 10 μmol/L, and hence would result in a correspondingly higher photonic efficiency. Using a concentration of a similarly high magnitude is not possible, as this is well outside of the experimental parameters, however when calculating the photonic efficiency at a concentration of 24 μmol/L, the experimental starting concentration, the calculated average photonic efficiency is much higher, at 0.4%, and this is with a doubling of concentration only. This implies that the photonic efficiency of this reactor may be on par if not comparatively higher than that achieved by Dionysiou et al. [26].

4.5. Improving SDR performance – mass transfer limitations

Taking into account the previous analysis, mass transport limitations are occurring. The key indicator of this is that the order of the reaction is different for a flow rate of 15 mL/s to the other employed flow rates. This is shown more clearly in Fig. 12a, when calculating the photonic efficiency at the start of the experiment, at 26 μmol/L, there is no obvious correlation in the photonic efficiency with the film height. However, when calculating it at half the starting concentration, 10 μmol/L (Fig. 12b), the calculated photonic efficiency for the 15 mL/s reactions is an order of magnitude higher as compared to the rest, indicating that some mass transfer effect must be affecting the reaction rate (as the irradiance is remaining constant). Consequently, future work will focus on increasing mixing and turbulence on the disc in order to eliminate the mass transfer perpetrated reaction rate drop.

5. Conclusions

It was found that the thin film photocatalytic SDR reduces photon transfer limitations, this is probably the result of the thickness of the film formed across the surface of the disc; with calculated average thicknesses between 160 and 450 μm. However, the wave regimes did not impact the reaction rate and mass transfer limitations are still occurring. The flow across the disc is laminar as shown by dye injection studies, and the wave regime did not have an effect on this. However, two reactions with much higher than expected conversions were observed at 15 mL/s and 100 and 200 rpm with pseudo-first order constants of 8.8 and 8.9×10^{-6} m/s respectively.

The other reactions followed pseudo-second order kinetics, suggesting that the switch in reaction order occurs due to a mass transfer limitation, most likely due to the laminar flow on the disc. The mechanism responsible for the significant enhancement in the reaction rates for the two pseudo-first order reactions will be investigated in future work.

Acknowledgements

The authors acknowledge the University of Auckland Doctoral Scholarship supporting Irina. The authors also acknowledge Allan Clendinning, Ray Hoffmann, Peter Buchanan, Laura Liang, Catherine Hobbis, Frank Quin and Tanya Groutso for technical help, the University of Auckland's Faculty of Engineering Workshop for fabricating the reactor and Emma Patterson for recruiting Simon and creating a great collaboration.

References

[1] A. Mills, S. Le Hunte, Journal of Photochemistry and Photobiology A: Chemistry 108 (1) (1997) 1–35.
[2] T. Van Gerven, G. Mul, J. Moulijn, A. Stankiewicz, Chemical Engineering and Processing 46 (9) (2007) 781–789.
[3] A.M. Ali, E.A. Emanuelsson, D.A. Patterson, Applied Catalysis B: Environmental 97 (1–2) (2010) 168–181.
[4] C. McFarlane, E.A.C. Emanuelsson, A. Ali, W. Gao, D.A. Patterson, International Journal of Chemical Engineering 2 (2010) 63–79.
[5] C. Brechtelsbauer, N. Lewis, P. Oxley, F. Ricard, C. Ramshaw, Organic Process Research & Development 5 (1) (2000) 65–68.
[6] A. Aoune, C. Ramshaw, International Journal of Heat and Mass Transfer 42 (14) (1999) 2543–2556.
[7] K.V.K. Boodhoo, R.J. Jachuck, Applied Thermal Engineering 20 (12) (2000) 1127–1146.
[8] A. Charwat, R. Kelly, C. Gazley, Journal of Fluid Mechanics 53 (2) (1972) 227–255.
[9] J.R. Burns, C. Ramshaw, R.J. Jachuck, Chemical Engineering Science 58 (11) (2003) 2245–2253.
[10] I. Tsibranska, D. Peshev, G. Peev, A. Nikolova, Chemical Engineering and Processing: Process Intensification 48 (3) (2009) 823–827.
[11] A.I. Butuzov, I.I. Pukhovoi, Journal of Engineering Physics and Thermophysics 31 (2) (1976) 886–891.
[12] H.C. Yatmaz, C. Wallis, C.R. Howarth, Chemosphere 42 (4) (2001) 397–403.
[13] H. Gnaser, M.R. Savina, W.F. Calaway, C.E. Tripa, I.V. Veryovkin, M.J. Pellin, International Journal of Mass Spectrometry 245 (2005) 61–67.
[14] C.M. Ling, A.R. Mohamed, S. Bhatia, Chemosphere 57 (7) (2004) 547–554, Times cited: 12.
[15] O. Carp, C.L. Huisman, A. Reller, Progress in Solid State Chemistry 32 (2004) 33–177.
[16] C.S. Turchi, D.F. Ollis, Journal of Catalysis 122 (1) (1990) 178–192.
[17] G.L. Puma, J. Khor, A. Brucato, Environmental Science & Technology 38 (13) (2004) 3737–3745.
[18] H. Espig, R. Hoyle, Journal of Fluid Mechanics 22 (4) (1965) 671–677.
[19] O.K. Matar, C.J. Lawrence, G.M. Sisoev, Physics of Fluids 17 (052102) (2005).
[20] M.A. Rauf, M.A. Meetani, A. Khaleel, A. Ahmed, Chemical Engineering Journal 157 (2010) 373–378.
[21] G. Leneweit, K.G. Roesner, R. Koehler, Experiments in Fluids 26 (1999) 75–85.
[22] N. Sakai, A. Fujishima, T. Watanabe, K. Hashimoto, Journal of Physical Chemistry B 107 (2003) 1028–1035.
[23] K. Thamaphat, P. Limsuwan, B. Ngotawornchai, Kasetsart Journal (Nature Science) 42 (2008) 357–361.
[24] A. Houas, H. Lachheb, M. Ksibi, E. Elaloui, C. Guillard, J.-M. Herrmann, Applied Catalysis B: Environmental 31 (2001) 145–157.
[25] A. Ghanadzadeh, A. Zeini, A. Kashef, M. Moghadam, Journal of Molecular Liquids 138 (2008) 100–106.
[26] D.D. Dionysiou, G. Balasubramanian, M.T. Suidan, A.P. Khodadoust, I. Baudin, J.-M. Laîne, Water Research 34 (11) (2000) 2927–2940.
[27] J. Tschirch, R. Dillert, D. Bahnemann, B. Proft, A. Biedermann, B. Goer, Research on Chemical Intermediates 34 (4) (2008) 381–392.